540. Fiberconcrete non-linear fracture control through fresh concrete flow numerical simulation

A. Krasnikovs[1,a], O. Kononova[1,b], A. Khabaz[1,c], J. Viba[1,d]
[1] Riga Technical University, Ezermalas 6, LV-1006, Riga, Latvia
e-mail: [a]*akrasn@latnet.lv,* [b]*olga.kononova@gmail.com,* [c]*khabbaz966@hotmail.com,* [d]*Janis.Viba@rtu.lv*
Phone: +371-67089473
(Received 27 January 2009; accepted 07 June 2010)

Abstract. The use of fiber (steel or synthetic) reinforced concrete (FRC) had a considerable increase during the last decades mainly due to its higher resistance to crack formation and simplified casting technique. At the same time fiberconcrete strength properties are non-linear with a high scatter. The paper presents results for fiberconcrete post-cracking behavior control by means of fresh FRC flow numerical simulations and prediction of internal structure (fiber orientation and distribution) formation.

Keywords: fiber reinforced concrete (FRC), crack forming, fiberconcrete strength, flow numerical simulation, internal structure

Introduction

While situation of unstable cracks propagation is acquired soon in loaded unreinforced concrete matrix, cracks can be bridged by fibers, in the case of FRC, and the material can carry loads far beyond the plain concrete matrix cracking. Such short fibers may be metallic – steel and non-metallic - glass, carbon and aramid. High tensile load bearing capacity requires large fiber percentage in the structure of material, what immediately leads to noticeable decrease of fresh FRC workability. In order to maintain a suitable workability, fiber percentage in the concrete mix is technologically limited. Traditionally fiber volume fraction does not exceed 4-5% and leads to high scatter of tensile post-cracking strength properties. Typical stress-deformation curve for FRC prism (15x15x60cm) under 4-point bending loading conditions is shown at Fig.1. It is important to predict and control crack opening and cracked beam load bearing capacity after the cracks formation ("plato" on the figure 1), when construction member deflections are measured by millimeters and all tensile loads are carried by fibers bridging the cracks [1,2].

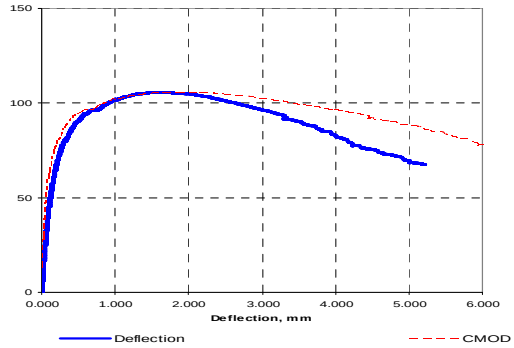

Fig. 1. Stress-midpoint deflection and crack mouth opening displacement (CMOD) diagrams for steel fiberconcrete (subjected to 4-point loading) with fiber content V_f equal to 2.9%

Fresh concrete properties monitoring by numerical simulation

Fresh FC is viscous (or highly viscous) liquid and its flow, filling of the mould or trench in the ground needs additional investigation. Fibers in fresh FRC during its transportation can obtain different orientation and spatial distribution. As a consequence it will change the place of weakest (having lowest number of crossing fibers and preliminary worst orientation) cross-section on the beam along its length.
This paper is devoted to:
a) numerical simulation of fiber spatial distribution in fiberconcrete construction member;
b) FRC flow modeling with the goal to recognize internal surface formation in the material, with major fiber orientations;
c) FRC flow modeling filling the mould as well as deep and narrow trench in the ground is creating under cut and cover tunneling technology (see Fig. 2).
Different authors performed fresh FC flow numerical simulation, observes FC as viscous single fluid, or fluid with discrete particles [3-7]. In our paper we are adapting single fluid FC model. FC flow computational modeling could be the potential instrument for understanding the rheological behavior of concrete simultaneously performing fibers orientation monitoring in concrete body and improving FC mix design. Numerical simulation of the casting process could allow civil engineers to specify a minimum FC workability that could ensure the proper filling of a given formwork.

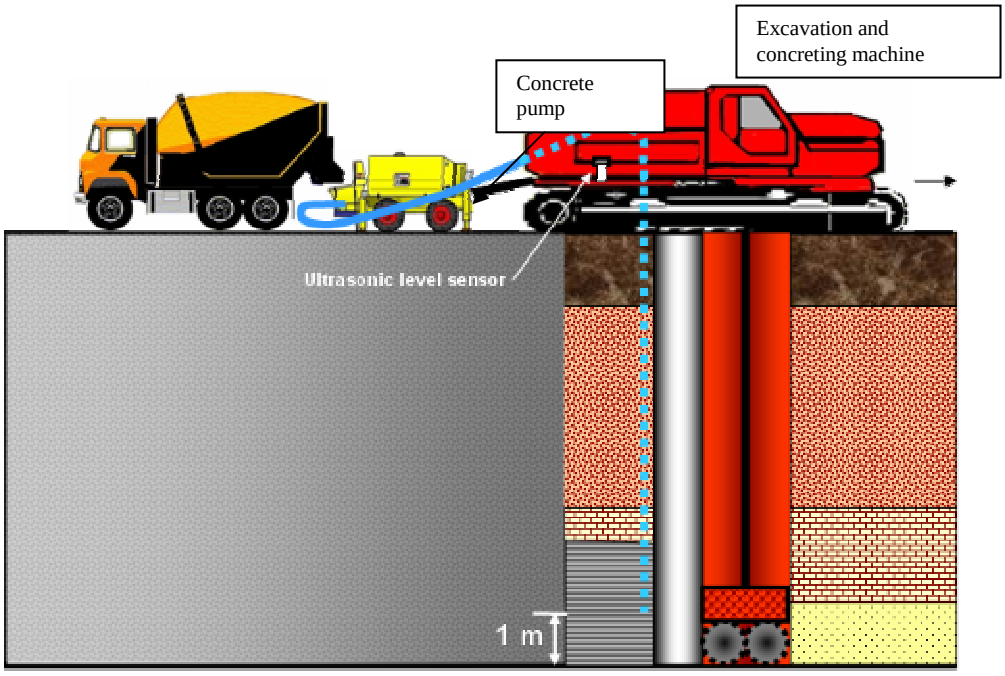

Fig. 2. Fresh FC filling into the ground trench (picture created by AITEMIN (Spain))

Fibers distribution simulation in FRC prism body

Simulations of fiber spatial positions and orientation distributions in FRC body were performed using probabilistic Monte - Carlo method. Simulations results were verified

experimentally. For each fiber in broken FRC cross-section (see Fig. 3. a.) was measured length of fiber part was pulled out of concrete during crack opening. Simulated and measured

Fig. 3. a) Crack surface with pulled out steel fibers

fiber lengths (length of fiber part was pulled out of concrete during crack opening) and spatial orientations (angle to crack surface) are presented in Fig.3b and c. Comparison of results of probabilistic simulations with experimental findings reveal high deviation in fiber orientations for experimentally measured samples and modeling results (was made with assumption of pure random parameters distribution). Conclusion can be made about weak surface formation with fibers mainly oriented parallel to surface plane. Reason may be in fibers orientation in viscous flow with velocity gradient (see Fig.4.) Numerical simulations using FEM were performed with the goal to detect positions of weak load bearing surfaces (along the FRC sample) as the surfaces with high velocities gradients in fresh FRC during mould filling. Fig. 5 provides velocity distributions during prism mould filling.

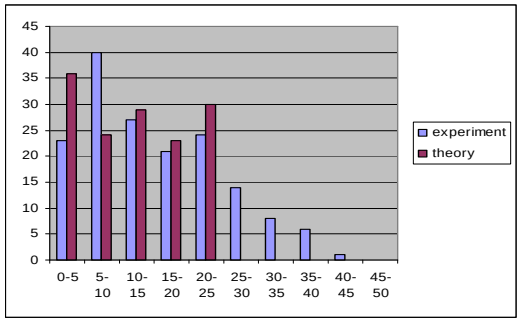

Fig. 3. b) Fibers length distribution in broken cross-section

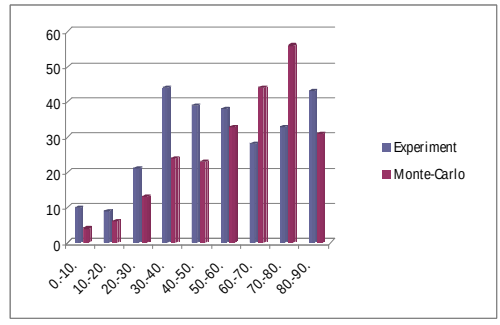

Fig. 3. c) Fibers angle to crack surface distribution in broken cross-section

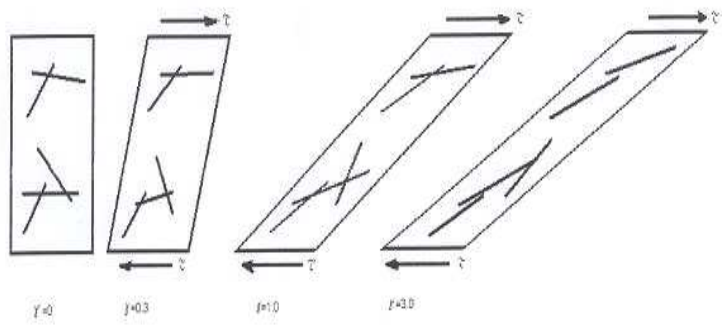

Fig. 4. Fibers orientation in viscous flow with velocity gradient

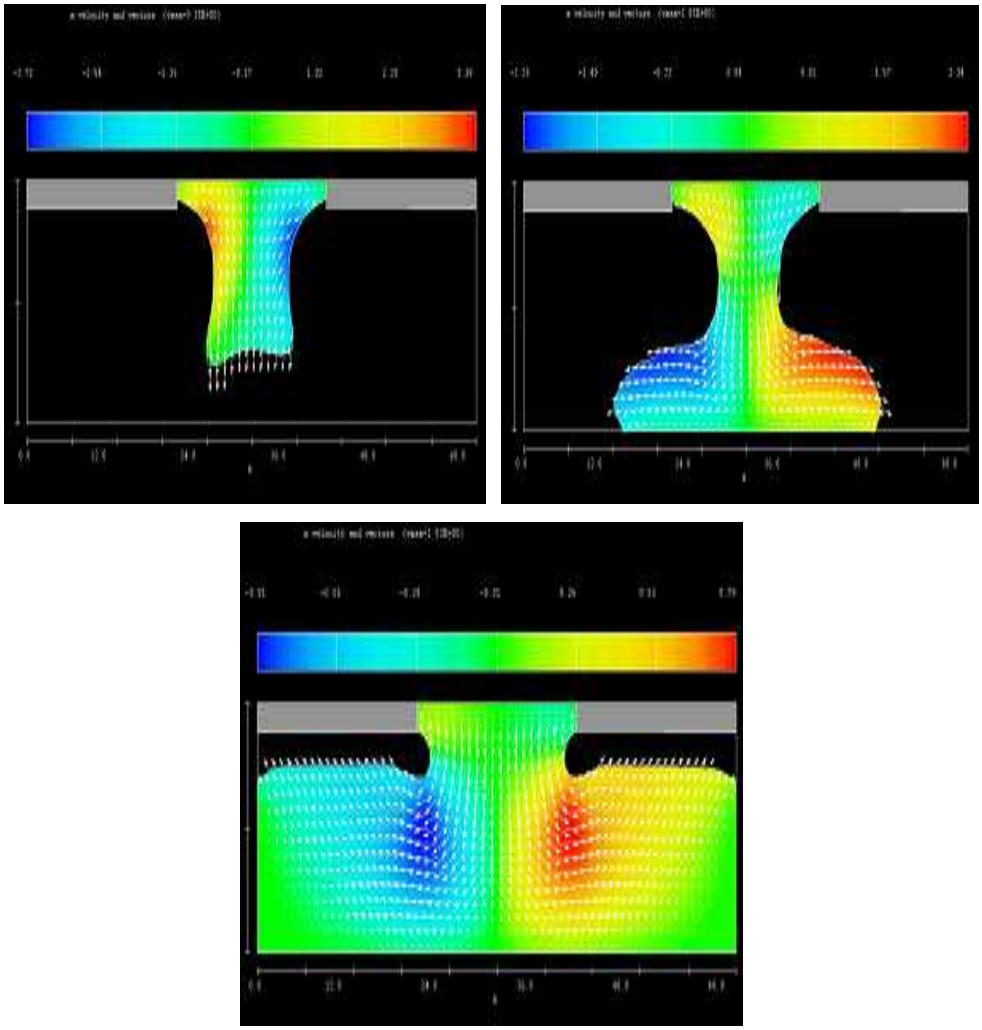

Fig. 5. Fibers velocities in viscous FRC flow during mould filling

High gradient areas along the mould were detected at the sides of central flow and FRC in the mould. Places of high gradients were compared with magistral crack location places obtained during strength tests. Good agreement was achieved.

Fibers distribution simulation in FRC tunnel membrane wall

FC is pumped by pump and throw tremie pipe is filling the trench from the bottom, during slow excavation machine motion forward, erecting concrete wall of the new tunnel (see Fig. 2.).

Viscous fluids plug motion in the pipe. Comparison of two methods: finite element (FLOW3D) and finite differences methods

FC can form plugs during its motion in the pipe. For investigation of this phenomenon a 2D numerical simulation using commercial finite element code FLOW 3D and finite difference methods was executed. Finite element and finite difference methods had Lagrangian integration points. Viscous incompressible fluid plug is in the pipe (see Fig. 6).

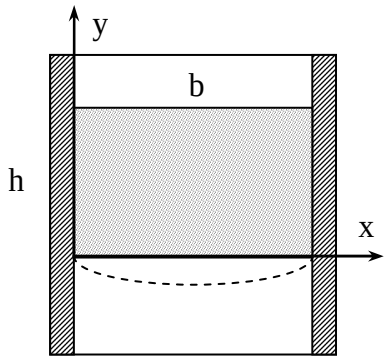

Fig. 6. Viscous fluid tap in the pipe

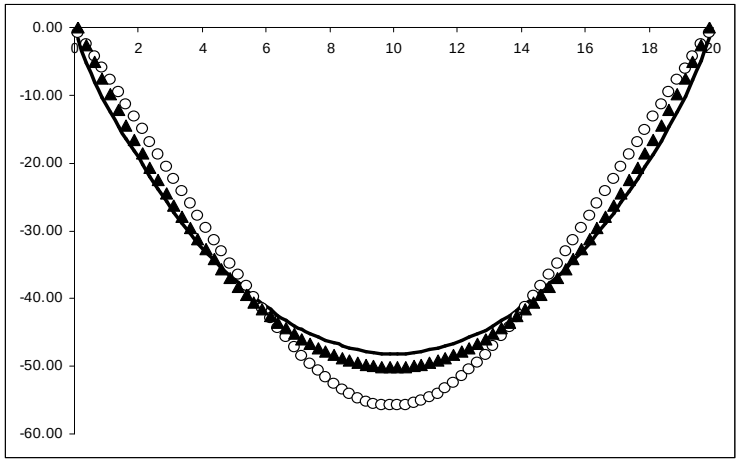

Fig. 7. Velocity distribution in the moving plug (calculations were done using finite elements method (FLOW3D) and finite differences method). ——— - velocity at the bottom surface (FLOW 3D); ○○○○○ - velocity at the top surface (FLOW 3D); ▲▲▲▲▲ - velocity (finite differences).

The following assumptions were adopted:

1. only vertical velocity v_y is observed;
2. flow is incompressible or v_y is not depending on y coordinate, but only on x coordinate;
3. in the vicinity of the walls the velocities v_y are equal to zero. The shear stress in wall vicinity is linearly proportional to the slip velocity. The coefficient of proportionality is the friction coefficient. When the friction coefficient is infinitely large the wall slip velocity is equal to zero.

Navier-Stokes equations for our case are [8]:

$$\begin{aligned}
\frac{dv_x}{dt} &= F_x - \frac{1}{\rho}\frac{\partial p}{\partial x} + \frac{\eta}{\rho}\left(\frac{\partial^2 v_x}{\partial x^2} + \frac{\partial^2 v_x}{\partial y^2} + \frac{\partial^2 v_x}{\partial z^2}\right), \\
\frac{dv_y}{dt} &= F_y - \frac{1}{\rho}\frac{\partial p}{\partial y} + \frac{\eta}{\rho}\left(\frac{\partial^2 v_y}{\partial x^2} + \frac{\partial^2 v_y}{\partial y^2} + \frac{\partial^2 v_y}{\partial z^2}\right), \\
\frac{dv_z}{dt} &= F_z - \frac{1}{\rho}\frac{\partial p}{\partial z} + \frac{\eta}{\rho}\left(\frac{\partial^2 v_z}{\partial x^2} + \frac{\partial^2 v_z}{\partial y^2} + \frac{\partial^2 v_z}{\partial z^2}\right).
\end{aligned} \quad (1)$$

where F_x ,F_y, F_z are the mass forces (for gravity F_y=-g, where g is free falling acceleration), p is pressure, η is a coefficient of dynamic viscosity, ρ is the fluid density.

In the case of the plug we have only one equation (under accepted earlier predictions). Here pressure is not depending on y coordinate and we have only one velocity component v_y. For our task have place the Lagrange reference frame and equations (1) acquire the following form:

$$\frac{dv_y}{dt} = F_y + \frac{\eta}{\rho}\frac{\partial^2 v_y}{\partial x^2}, \quad (2)$$

Using finite differences method, the partial differential equation (2) is rewritten as follows:

$$\frac{1}{\tau}\left(v_{t+1,x} - v_{t,x}\right) = -g + \frac{\eta}{\rho h^2}\left(v_{t,x+1} - 2v_{t,x} + v_{t,x-1}\right), \quad (3)$$

Numerical calculation results according to formulae (3) with above-mentioned boundary conditions were compared with the results obtained using finite element method code *FLOW-3D*®. Velocity distribution comparison is illustrated in Fig.7. It is necessary to mention that finite differences model in (3) interpretation is giving the same velocities for the points that are located on the lines parallel to the pipe axle. In this sense we observe good correlation between both numerical methods. Looking at velocities profiles in FRC plug is moving in the pipe, it is possible to observe areas of high velocity gradients between central core of the plug and pipe walls. Fibers in these areas tend to obtain orientation parallel to pipe longitudinal axis. This effect is stronger for longer pipes.

FC flow numerical modeling for the case of filling deep and narrow trench in the ground

Literature provides different rheological models that describe the relation between the shear stress τ and the shear strain rate $\dot{\gamma}$ in cement-based materials. Two of them, namely Newton's and Bingham's models, were used in our investigation. The simplest is the Newton viscous fluid model [9]:

$$\tau = \eta \dot{\gamma} , \quad (4)$$

Newton model successfully describes very flow able FC flow (such as was observed for self compacting concretes (SCC)). Increasing fiber content (or using non-SC concretes), material is obtaining τ_0 – motion starting yield stress, below which fresh FC is staying in stable state. In this case we can use Bingham's model:

$$\begin{aligned} &\tau = \tau_0 + \eta\dot{\gamma} \quad if \quad \tau \geq \tau_0 \\ &\dot{\gamma} = 0 \quad if \quad \tau \leq \tau_0 \end{aligned} , \quad (5)$$

where τ_0 – is the mentioned yield stress. When applied shear stresses do not exceed the yield stress, the material behaves as a solid. Once the yield stress is exceeded, however, the material is obtaining the viscous fluid mechanical properties.
In the framework of *FLOW-3D*® the stiffness of a Bingham material below its yield point was evaluated using such approach: the yield stress in this case is the shear stress is reaching at some limiting strain rate, at higher strain rates, the material is obtaining a much lower viscosity. The initial viscosity and the value of the limiting rate-of-strain can control the interval where the stress is below the yield stress. Above the yield point the slope of the shear - stress versus strain-rate curve is consistent with a much lower viscosity.
Since shear stress is equal to viscosity times the strain rate, we can easily derive the viscosity function needed to generate the approximate Bingham-stress versus strain-rate curve. The non-Newtonian viscosity model in *FLOW-3D*® has all the necessary features for this approximation.

Flow parameters and results

Comprehensive parametric study was performed investigating pressure and local velocity (local fiber orientations are dependant on local FC flow velocities) in different places of the system depending on trench and pipe geometry, excavating machine motion velocity and pump pressure value [10]. Calculation results are shown in Fig.8-13. In this case trench size is 5 m deep and 2 m long. Internal size of pipe cross-section is 20 cm, pump pressure $2{,}026*10^6$ dyne/cm^2 (2 atm), horizontal velocity of the excavation machine is 0,5 cm/sec (in the case of calculation made for Newton fluid) and 0,15 cm/sec (for Bingham fluid). Concrete density is 2400 kg/m^3, coefficient of viscosity 500 Pa·sec and yield stress 500 Pa. Vertical and horizontal dimensions (largest) of finite elements are 3 cm. The number of finite elements is 13400. The total pumping time is 240 sec for Newton fluid and 815 s for Bingham fluid model (for the case under consideration).
Looking in Fig.8 and 9 we observe that at the beginning of pumping Bingham fluid (comparing with Newton's one) has lower pumpability. Higher pressure and longer time is required to pump the same liquid volume into the trench. When flow is stabilized (see Fig.10 and 11)

© VIBROMECHANIKA. JOURNAL OF VIBROENGINEERING. 2010, JUNE, VOLUME 12, ISSUE 2, ISSN 1392-8716

pressure distributions in the systems become very similar despite that in the same time velocities of trench filling are quite different.

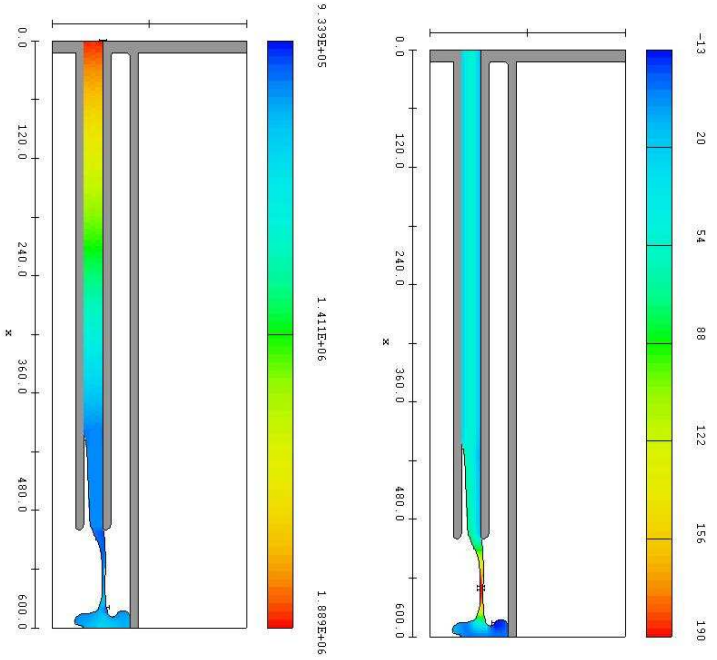

Fig. 8. Pressure (a) and local velocity (b) in the concrete at time moment t=10,5 sec (from the beginning of pumping) (Newton's fluid model)

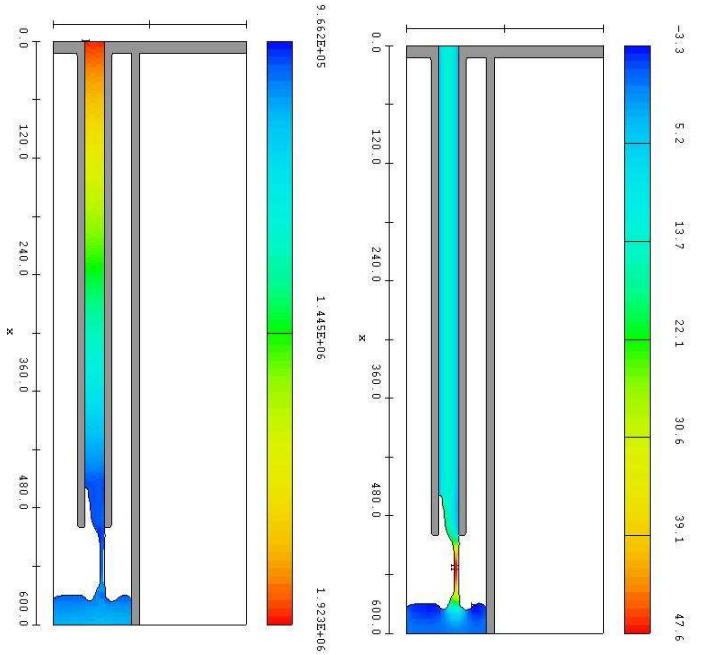

Fig. 9. Pressure (a) and velocity (b) in Bingham's model, t=40 sec

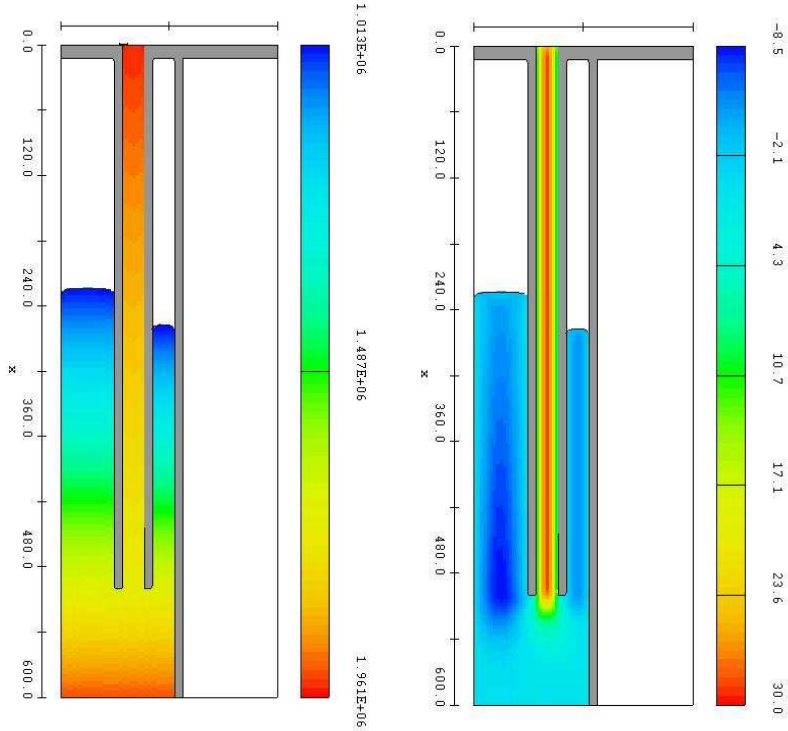

Fig. 10. Pressure (a) and velocity (b) in Newton's model, t=60,1 sec

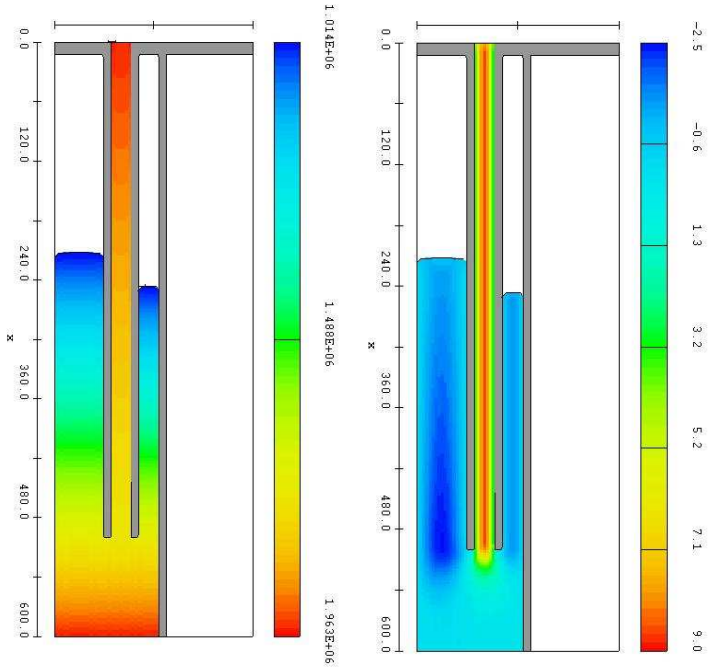

Fig. 11. Pressure (a) and velocity (b) in Bingham's model, t=200,1 sec

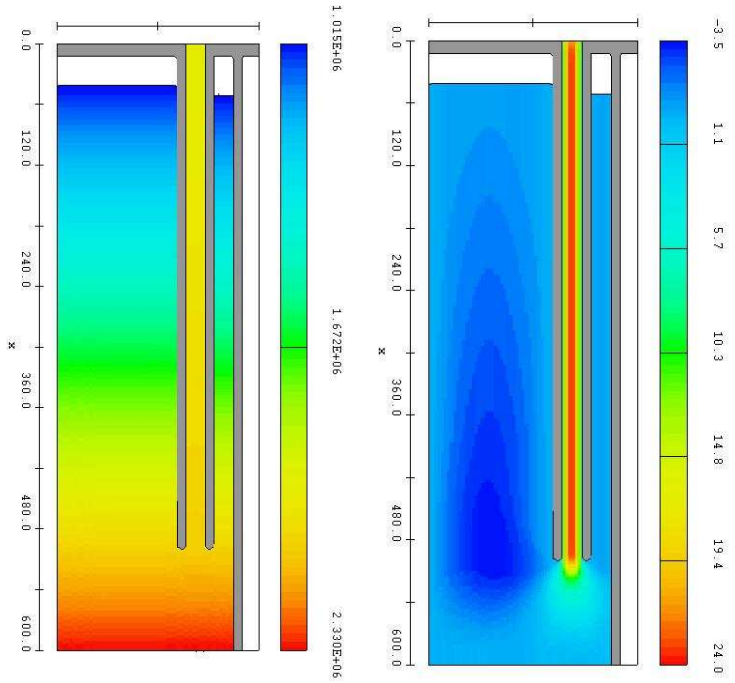

Fig. 12. Pressure (a) and velocity (b) in Newton's model, t=200,5 sec

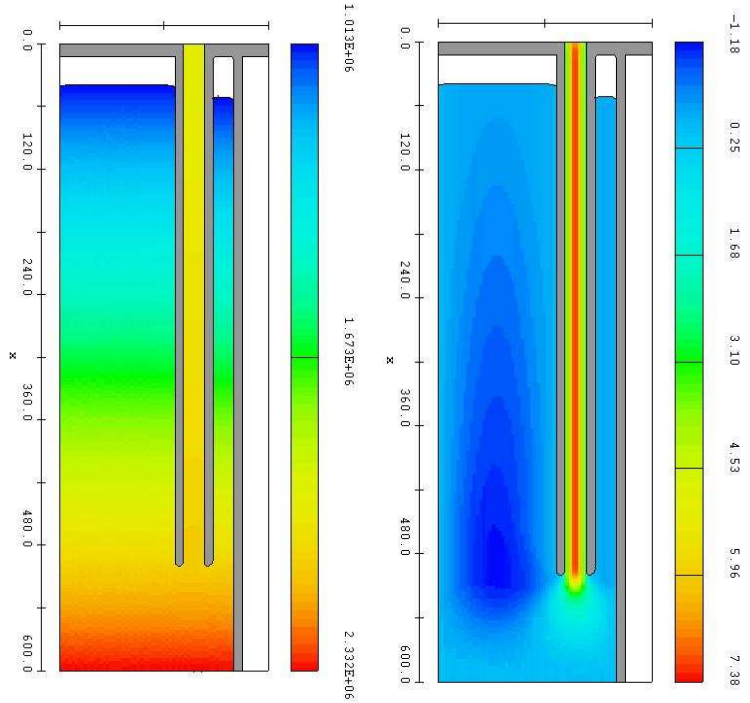

Fig. 13. Pressure (a) and velocity (b) in Bingham's model, t=610,1 sec

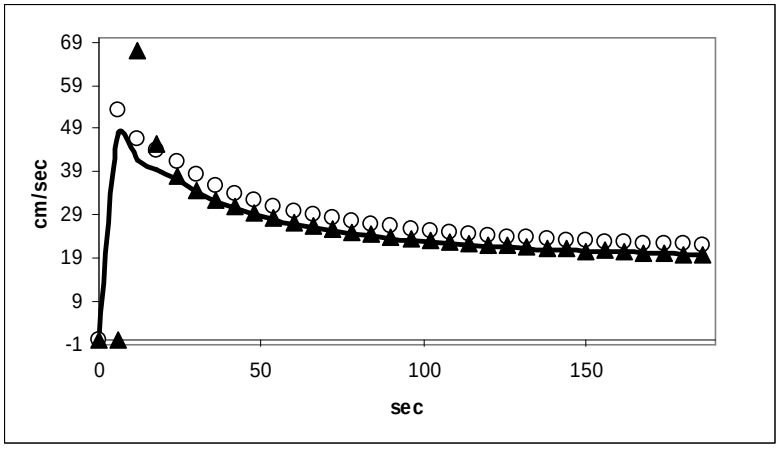

Fig. 14. Velocities in the fiberconcrete during the pumping (Newton's fluid model) ——— - velocity at the top point of the pipe; ○○○○○○ - velocity in the middle point of the pipe; ▲▲▲▲▲▲ - velocity at bottom point of the pipe.

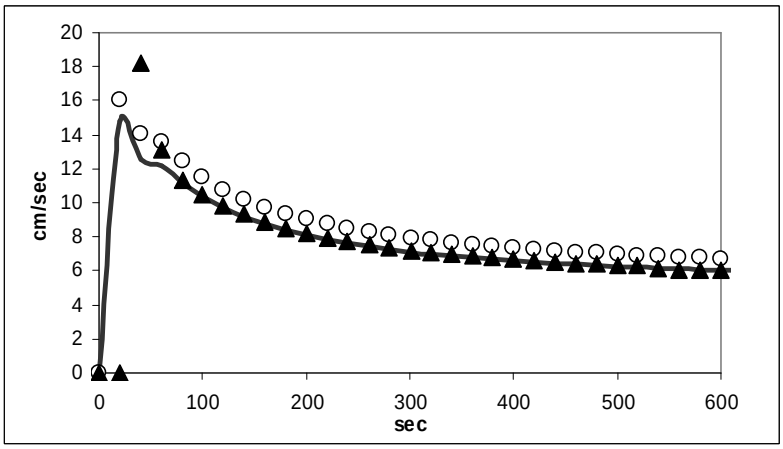

Fig. 15. Velocities in the fiberconcrete during the pumping (Bingham's fluid model) ——— - velocity at the top point of the pipe; ○○○○○○ - velocity in the middle point of the pipe; ▲▲▲▲▲▲ - velocity at bottom point of the pipe.

Majority of fibers in the pipe cross-section are (approximately) oriented in flow direction. These become more pronounced for the lower part of the pipe. Fibers with concrete going out of the bottom end of the pipe are filling the bottom part of the trench and are lifting up upper layers of fiberconcrete. At the same time excavation machine motion forward leads to formation of the volume with opposite flow direction in the central part of concrete wall body (see. Fig.10b-13b). Fibers in this concrete volume are rotating and depending on machine motion velocity and pipe diameter and pump pressure can form areas with dominant orientation in horizontal direction. This phenomena cal lead to formation of the belt with weak load bearing capacity concerning to cylindrical bending around horizontal axis in the wall body.

Conclusions

Fiberconcrete structure formation (distributions and orientations of fibers) wase investigated experimentally and numerically. With the goal of determination of weak load bearing surfaces, real ground tunnel membrane wall concreting with moving excavating and concreting combine was numerically observed. Fiberconcrete flow simulations were performed using different numerical methods. Two concrete flow models, namely Newton and Bingham, were applied with subsequent comparison of obtained results. Simulations revealed that fiberconcrete wall can obtain areas with weak bending resistance in vertical plane according to dominant fiber orientations in these areas. At the same time performing mathematical concreting parameters (combine motion velocity, pump pressure, tremie pipe position during concreting, concrete viscosity) optimization is possible in order to avoid such situation and obtain membrane wall with the highest bending resistance capacity.

REFERENCES

[1] **Kononova O., Pupurs A., Krasnikovs A.** *Fiber concrete beam failure observed as rare phenomena.* Journal of Vibroengineering, December 2008, Volume 10, Issue 4, 497-499.

[2] **Krasnikovs A., Kononova O.** *Strength prediction for concrete reinforced by different length and shape short steel fibers.* Scientific Proceedings of Riga Technical University Transport and Engineering 6, Volume 31, Riga 2009, 89-93

[3] **Roussel N., Geiker M. R., Dufour F., Tharane L. N., Szabo P.** *Computational modeling of concrete flow: General overview.* Cement and Concrete Research 37, (2007) 1298 – 1307.

[4] *Numerical modelling of concrete flow: homogeneous approach.* International journal for numerical and analytical methods in geomechanics, Int. J. Numer. Anal. Meth. Geomech., 2005; 29:395–416.

[5] **Yakinthos K., Vlahostergios Z., Goulas A.** *Modeling the flow in a 90^0 rectangular duct using one Reynolds-stress and two eddy-viscosity models.* International Journal of Heat and Fluid Flow 29, (2008) 35-47.

[6] **Barletta A.** *Parallel and non-parellel laminar mixed convection flow in an inclined tube: The effect of the boundary conditions.* International Journal of Heat and Fluid Flow 29, (2008) 83-93.

[7] **Hall O., Hills C. P., Gilbert A. D.** *Slow flow between concentric cones.* The quarterly journal of mechanics and applied mathematics. Volume 60, Part 1. February 2007, 27-48.

[8] **Валландер, Сергей.** Лекции по гидроаэромеханике. Издательство ЛГУ 1978.

[9] **Malkin A. Ya., Isayev A. I.** Rheology: conceptions, methods, applications. ChemTec Publishing, 2005.

[10] **Kononova O., Krasnikovs A., Eiduks M.** *Fiber concrete viscous flow numerical simulation.* Scientific Proceedings of Riga Technical University Transport and Engineering 6, Volume 28, Riga 2008, 121-131.